OPEN

A Single-Arm, Multicenter Validation Study of Prostate Cancer Localization and Aggressiveness With a Quantitative Multiparametric Magnetic Resonance Imaging Approach

Marnix C. Maas, PhD, Geert J.S. Litjens, PhD,* Alan J. Wright, PhD,† Ulrike I. Attenberger, MD, PhD,‡
Masoom A. Haider, MD, FRCPC,§ Thomas H. Helbich, MD, MBA,|| Berthold Kiefer, PhD,¶
Katarzyna J. Macura, MD, PhD,# Daniel J.A. Margolis, MD, PhD,** Anwar R. Padhani, MB, BS,††
Kirsten M. Selnæs, PhD,‡‡ Geert M. Villeirs, MD, PhD,§§
Jurgen J. Fütterer, MD, PhD,* and Tom W.J. Scheenen, PhD**

Objectives: The aims of this study were to assess the discriminative performance of quantitative multiparametric magnetic resonance imaging (mpMRI) between prostate cancer and noncancer tissues and between tumor grade groups (GGs) in a multicenter, single-vendor study, and to investigate to what extent site-specific differences affect variations in mpMRI parameters.

Materials and Methods: Fifty patients with biopsy-proven prostate cancer from 5 institutions underwent a standardized preoperative mpMRI protocol. Based on the evaluation of whole-mount histopathology sections, regions of interest were placed on axial T2-weighed MRI scans in cancer and noncancer peripheral zone (PZ) and transition zone (TZ) tissue. Regions of interest were transferred to functional parameter maps, and quantitative parameters were extracted. Across-center variations in noncancer tissues, differences between tissues, and the relation to cancer grade groups were assessed using linear mixed-effects models and receiver operating characteristic analyses.

Results: Variations in quantitative parameters were low across institutes (mean [maximum] proportion of total variance in PZ and TZ, 4% [14%] and 8% [46%], respectively). Cancer and noncancer tissues were best separated using the diffusion-weighted imaging-derived apparent diffusion coefficient, both in PZ and TZ (mean [95% confidence interval] areas under the receiver operating characteristic curve [AUCs]; 0.93 [0.89–0.96] and 0.86 [0.75–0.94]), followed by MR spectroscopic imaging and dynamic contrast-enhanced-derived parameters. Parameters from all imaging methods correlated significantly with tumor grade group in PZ tumors. In discriminating GG1 PZ tumors from higher GGs, the highest AUC was obtained with apparent diffusion coefficient (0.74 [0.57–0.90], $P < 0.001$). The best separation of GG1–2 from GG3–5 PZ tumors was with a logistic regression model of a combination of functional parameters (mean AUC, 0.89 [0.78–0.98]).

Conclusions: Standardized data acquisition and postprocessing protocols in prostate mpMRI at 3 T produce equivalent quantitative results across patients from multiple institutions and achieve similar discrimination between cancer and noncancer tissues and cancer grade groups as in previously reported single-center studies.

Key Words: prostate cancer, Gleason group, mpMRI, quantitative validation, multicenter, interpatient variation, intersite variation

(Invest Radiol 2019;54: 437–447)

P rostate cancer (PCa) is the second most frequently diagnosed noncutaneous malignancy in men in the world.[1] Accurate localization of the disease within the organ is of essential clinical importance, as it aids in directing targeted biopsies, improves preoperative staging, and can guide local therapies. Currently, prostate multiparametric magnetic resonance imaging (mpMRI) provides the best visualization of the prostate compared with other imaging methods.[2,3] This imaging examination consists of triplanar high-resolution T2-weighted (T2w) imaging, as well as various combinations of functional imaging methods, most importantly diffusion-weighted imaging (DWI), T1-weighted dynamic contrast-enhanced (DCE) imaging, and/or MR spectroscopic imaging (MRSI). It has shown promising results in PCa detection in many single-center and multicenter studies[4–6] and is recommended in international guidelines for several indications in PCa management.[7,8]

Interpretation of mpMRI is based on a qualitative evaluation of the different functional techniques of the examination. Although standardized scoring and reporting systems were used in large studies,[4,5] interobserver agreement between radiologists from different institutions remains only moderate.[9] Quantitative evaluation of mpMRI holds the potential to improve interobserver agreement and the possibility to compare or pool results between centers. It may allow defining objective decision thresholds and measures for diagnosis or assessment of aggressiveness, and may simplify the development of machine learning tools to help radiologists interpret the large amount of information inherent to mpMRI. However, the wide variety of acquisition and postprocessing protocols supported by current guidelines[10,11] leads to large additional variations in quantitative parameter values on top of true biological variability, limiting their applicability. For instance, in DWI, the maximum chosen b-value and the maximum attainable magnetic field gradient dictate the timing and amplitude of

the diffusion-encoding gradient pulses, which in turn influence the value of the calculated apparent diffusion coefficient (ADC). In DCE-MRI, the choice of contrast agent, injection rate, temporal resolution, and postprocessing protocol all influence the resulting parameter values,[12] and in MRSI, pulse sequence timing, magnetic field strength, and postprocessing models dictate the shape of the spectra and the accompanying values for metabolite ratios.

One approach to mitigate this issue is standardization. Although this would eliminate variations due to differences in the image formation protocols, interinstitutional variations may still remain due to machine-related and population differences. The purpose of this study was therefore to investigate to what extent site-specific differences affect variations in quantitative prostate mpMRI parameters obtained with highly standardized acquisition and postprocessing protocols, and to validate their discriminative performance between PCa and noncancer tissues and tumor grade groups in a multicenter study.

MATERIALS AND METHODS

This prospective multicenter study was performed as part of the Prostate Cancer localization with a Multiparametric MR Approach trial (PCAMAP, Clinicaltrials.gov identifier NCT01138527) and was overall approved by our institutional review board, as well as by all review boards (Health Insurance Portability and Accountability Act-compliant for US sites) of participating institutions. The principal institution (Radboud University Medical Center, Nijmegen, the Netherlands) was financially sponsored for this work by Siemens Healthcare (Erlangen, Germany). Those authors who are not employees of or consultants for Siemens Healthcare had control of inclusion of any data and information that might present a conflict of interest for those authors who are employees of or consultants for Siemens Healthcare.

Patients

This study aimed to include 10 patients prospectively and consecutively recruited at 5 institutions able to contribute data to the PCAMAP trial. With one of the institutions withdrawing from the study after 8 patients, the remaining 2 were consecutively included from one other contributing institution. Patients were included between June 2010 and March 2012. All patients had biopsy-proven PCa as determined by 10- to 12-core transrectal ultrasound-guided biopsies, no history of therapy to the prostate or other pelvic organs or androgen deprivation therapy, they were scheduled for radical prostatectomy with whole-mount or quartile-divided histopathology of the resected prostate, and written informed consent was obtained from each. An overview of patient characteristics is presented in Table 1.

TABLE 1. Patient and Tumor Characteristics

Institution		A	B	C	D	E	Overall
Number of patients		10	10	12	10	8	50
PSA, ng/mL*		4.7 [2.6–9.2]	9.0 [1.9–11.2]	9.3 [5.3–19.2]	6.0 [4.5–8.7]	5.9 [3.1–17.3]	6.5 [1.9–19.2]
Age, y*		63 [46–71]	63 [58–73]	60 [52–69]	58 [48–67]	64 [50–71]	62 [46–73]
Time between biopsy and MR examination (median/minimum days)							62/15
Time between MR examination and surgery (median/maximum days)							25/108
Pathologic stage†							
T2		6	7	4	7	6	30
T3		4	3	7	3	2	19
T4				1			1
Gleason Grade†	Number of tumors > 0.5 cm³						
PZ	Grade Group						
3 + 2	1			1			1
3 + 3	1	2		5	1	6	14
3 + 4	2	3	3	4	4	1	15
4 + 3	3	2	4	1	4		11
4 + 4	4	1				1	2
4 + 5	5		1			1	2
Unknown					2		2
Total		8	7	12	9	11	47
TZ	Grade Group						
1 + 2	1			1			1
2 + 3	1			1			1
3 + 2	1			1			1
3 + 3	1	4				1	5
3 + 4	2		2		3		5
4 + 5	5			1			1
5 + 3	4	1					1
Unknown					3		3
Total		5	2	4	6	1	18

*Numbers are medians; values between brackets indicate the range of observed values.

†Pathologic stage and Gleason grades were determined postoperatively.

MR indicates magnetic resonance; PZ, peripheral zone; TZ, transition zone; PSA, prostate specific antigen.

TABLE 2. MR Acquisition Parameters

	T2w TRA	T2w SAG	T2w COR	DWI	MRSI	DCE
Sequence	TSE	TSE	TSE	SS-SE-EPI	PRESS	TWIST
TR, ms	4000	4000	4000	3300	750	3.85
TE, ms	101	101	101	60	145	1.42
Acc. factor	2	2	2	2		2
Resolution, mm	0.6×0.6	0.6×0.6	0.6×0.6	2.2×1.6	Nominal, $7 \times 7 \times 7$ mm; true spherical volume, 1.0 cm^3	1.6×1.6
Slice thickness, mm	3	3	3	3.6		3.6
Slice distance, mm	3.6	3.6	3.6	3.6		3.6
Sequence-specific				b-values 0, 100, 400, 800 s/mm^2		Temporal resolution 4 s
TA	04:10	03:46	03:38	04:34	08:14	05:02

MR indicates magnetic resonance; DWI, diffusion-weighted imaging; TSE, turbo spin-echo; MRSI, magnetic resonance spectroscopic imaging; DCE, dynamic contrast-enhanced imaging; SS-SE-EPI, single-shot spin-echo echo planar imaging; PRESS, point-resolved spectroscopy; TWIST, time resolved with stochastic trajectories[13]; TR, repetition time; TE, echo time; TA, acquisition time; T2w, T2-weighted imaging; TRA, transverse; SAG, sagittal; COR, coronal; Acc., acceleration.

Magnetic Resonance Imaging and Postprocessing

All imaging was performed on 3 T MR systems (MAGNETOM Trio Tim, 4 institutions; MAGNETOM Verio, 1 institution; Siemens Healthcare, Erlangen, Germany), all running software version Syngo MR B17. Bowel preparation was performed according to local guidelines at each institution and could include injection of scopolamine butyl bromide and/or glucagon, or filling the rectum with ultrasound gel. All institutions used identical scanning protocols with spine and body array coils for signal reception and no endorectal coil. Anatomical T2w imaging, DWI, 3D spectroscopic imaging (MRSI), and DCE-MRI were acquired (Table 2). All postprocessing of MR data were performed centrally. From DWI data, ADC maps were calculated using the scanner software, including all b-values. All MRSI spectra were quality checked (QC) using an automated procedure[14] and preprocessed and fitted using a linear combination of model files (LCModel[15]) into maps of the integral ratios of relevant prostate metabolites choline (Cho), spermine (Spm), creatine (Cre), and citrate (Ci): (Cho + Spm + Cre)/Cit [CSC/C], Cho/(Spm + Cre) [C/SC], and Cho/(Spm + Cre + Cit) [C/SCC]. Dynamic contrast-enhanced MRI was analyzed semiquantitatively into maps of curve-descriptive parameters: initial area under the contrast enhancement curve (iAUC), relative enhancement (RE), washin (WI), and washout (WO).[16] This was done using in-house developed software implemented in MeVisLab (MeVis Medical Solutions, Bremen, Germany). If organ motion was observed between scans, rigid registration was performed between native functional images (ie, the b = 0 image in case of DWI and the first volume of DCE) and the corresponding transverse T2w image, and the same transform was applied to the parametric maps.

Histopathologic Examination

Histopathology was performed on the excised prostates according to the local protocol at each institution, and included at least fixation and hematoxylin and eosin staining of whole-mount axial tissue sections throughout the prostate. Prostates were cut approximately perpendicularly to the rectal wall to facilitate spatial matching to the MRI. Each local pathologist outlined the presence and extent of cancer tissue either on photographs of tissue sections or photographs of microscopy slides. The localized Gleason score of tumor tissue was indicated and classified according to the ISUP grading system for PCa,[17] in which grade groups (GGs) 1 to 5 are defined as follows: GG1, Gleason score ≤6; GG2, Gleason score 3 + 4 = 7; GG3, Gleason score 4 + 3 = 7; GG4, Gleason scores 4 + 4 = 8, 3 + 5 = 8, and 5 + 3 = 8; GG5, Gleason scores 9–10.

Annotation and Analysis of Regions of Interest

Regions of interest (ROIs) were placed on axial T2-weighed MRI scans in noncancer peripheral zone (PZ), noncancer transition zone (TZ), PZ cancer, and TZ cancer using whole-mount histopathology sections as reference, treating tumors as TZ cancers if at least 70% of their volume was in the TZ.[18] This was done by an MR physicist (M.C.M., 6 years' experience in prostate MRI) and a radiologist (J.J.F., 11 years' experience in prostate MRI) in consensus, using anatomical landmarks to establish correspondence between histopathology and imaging while being blinded to any functional imaging results. A maximum of 4 ROIs were selected per tissue type in each patient, corresponding to a theoretical maximum number of 16 ROIs per patient. Cancer lesions were only included if they were 0.5 cm^3 or larger and their Gleason score was known.[19] Regions of interest were constructed from MRSI voxels, as this method had the lowest spatial resolution, in the following manner (see Fig. 1). First, an MRSI voxel (red rectangles in middle column) was selected on the spectroscopic grid (blue lines) at a location maximally occupied by the intended tissue (top row: noncancer PZ; middle row: noncancer TZ; bottom row: PZ cancer). Subsequently, up to 6 directly neighboring MRSI voxels (left-right, anterior-posterior, superior-inferior) were selected, provided that they covered at least 50% of the same tissue (yellow rectangles). Each selected MRSI voxel was used in a single ROI only. Corresponding imaging voxels were selected by expanding each selected MRSI voxel to its true shape and size, a sphere of approximately 1 cm^3, induced by the weighted k-space sampling scheme and filtering used.[20] Finally, the shape of the spheres was adapted such that they only contained imaging voxels within the tissue of interest (Fig. 1, red and yellow outlines in right column). Within each resulting shaped sphere, histogram analysis was performed for each imaging parameter and the 25th percentile of parameters tending to decrease in cancer tissue (ie, ADC, WO) and the 75th percentile of parameters tending to increase in cancer tissue (all other parameters) were determined. Analogous to previous work,[21] one number was extracted from each multisphere ROI for each parameter, from the sphere with the most deviating values of that parameter (Fig. 1): the lowest 25th percentile ADC; the highest CSC/C, C/SC, and C/SCC; the highest 75th percentile iAUC, RE, and WI; and the lowest 25th percentile WO. Regions of interest were excluded from analysis of a particular parameter if the corresponding MRI data were not acquired, if the ROI showed obvious signs of postbiopsy hemorrhage on precontrast T1-weighted images, or suffered from artifacts such as distortions (DWI), insufficient quality (MRSI), or organ motion (DWI or DCE). Region of interest placement and
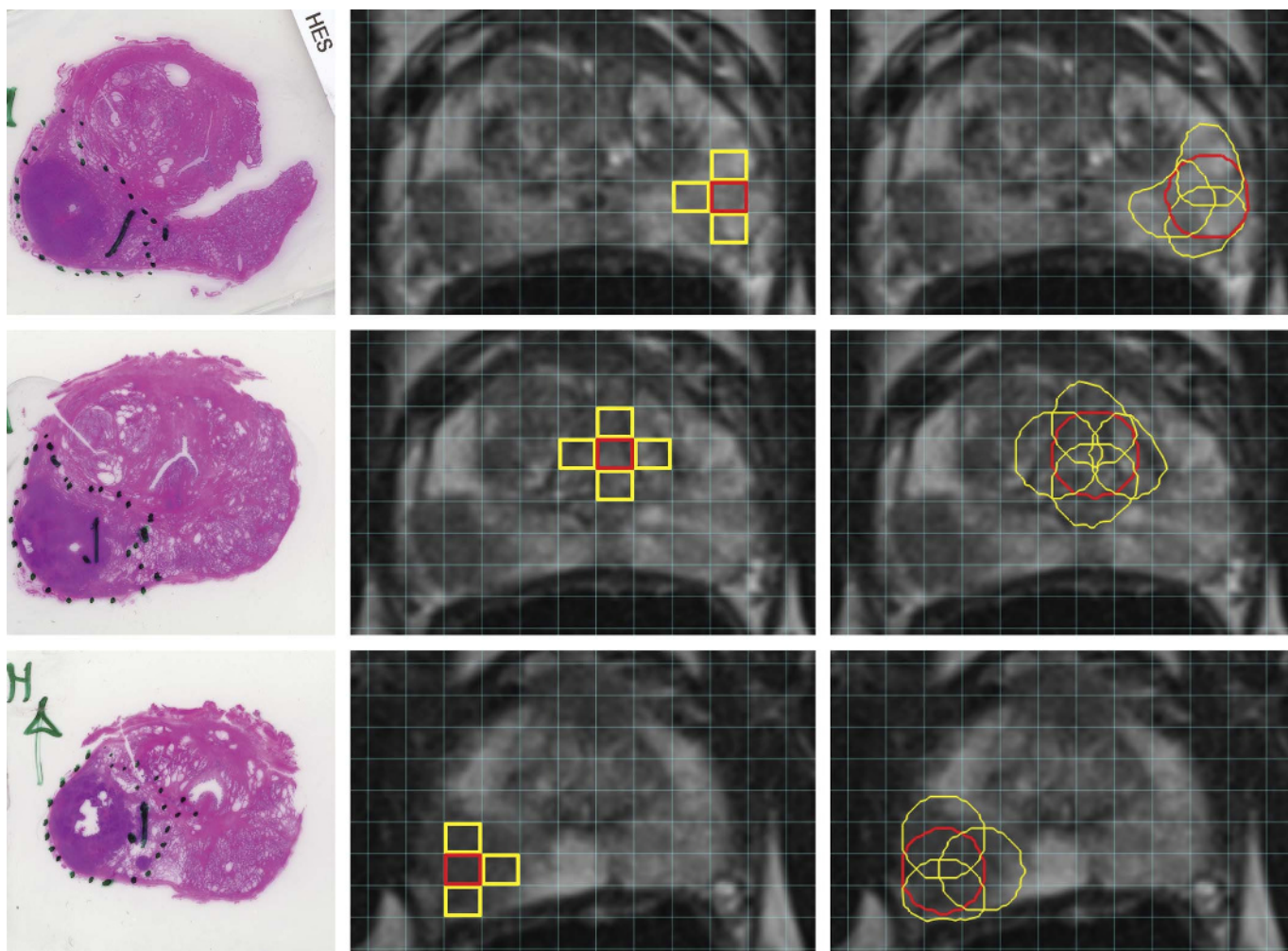
FIGURE 1. Example of the annotation of 3 ROIs in a 71-year-old man with a Gleason 3 + 4 prostate carcinoma in the right peripheral zone. Left column: Hematoxylin-eosin–stained histology slices at 3 different levels between midgland and apex (top to bottom), with the tumor outlined by the pathologist. Middle column: selection of primary MRSI voxels in noncancer PZ, noncancer TZ, and PZ cancer tissue (red rectangles in top, middle, and bottom rows), as well as up to 6 directly neighboring MRSI voxels (left-right, anterior-posterior, and superior-inferior, yellow rectangles). Neighboring voxels were only selected if they included the tissue of interest for at least 50%. Right column: selection of corresponding imaging voxels by expanding each selected MRSI voxel to a sphere representative of its true size (ie, ~1.0 cm^3), and adapting the shape of the spheres to only include the tissue of interest. For each parameter map, only one sphere per ROI, that is, the sphere with the most deviating values, was used for further analysis.

analysis was performed using a workstation developed in-house in MeVisLab (MeVis Medical Solutions, Bremen, Germany).

Statistical Analysis

Variations of functional parameter values between institutions and patients were quantified using a variance components analysis (VCA), in which the total variation observed in each parameter was decomposed into "between-institution," "between-patient," and "other" variations (ie, within-patient variations and measurement fluctuations), modeling institutions and patients as random main factors. This was done in noncancer tissues only to avoid any influence of population differences in, for example, tumor stages or grades on the results. Outliers were removed for this analysis, as these can have a disproportionate influence on sample variances as well as estimates of their separate components.[22] This was done according to Tukey's Fences method, removing points > 1.5 times the interquartile range (IQR) below the 25th percentile or above the 75th percentile of the pooled data distribution per tissue type and parameter map from the analysis. Outliers were removed in the VCA only; all

subsequent analyses were performed using all data that passed quality control. From the VCA, the proportion of variance (POV) attributable to each of the 3 factors (institutions, patients, other) was calculated for each parameter.

Differences between cancer and noncancer tissues in each parameter were analyzed separately for PZ and TZ using linear mixed models with "malignancy" as a fixed factor and "patient" as a random factor, accounting for multiple ROIs within one patient. A *P* value less than 0.05 was considered statistically significant. The ability of each parameter to discriminate between cancer and noncancer tissues was assessed using receiver operator characteristic (ROC) analyses, and confidence intervals of the areas under the ROC curves (AUCs) were calculated accounting for within-patient correlations using patient-level bootstrapping with 10,000 iterations.

Associations between quantitative mpMRI parameters and tumor aggressiveness were only analyzed in the PZ due to the low number of TZ tumors. Correlations between quantitative parameters and tumor grade group were calculated with Spearman correlation coefficients, and differences between tumor GG1 and GG2–5 as well as between
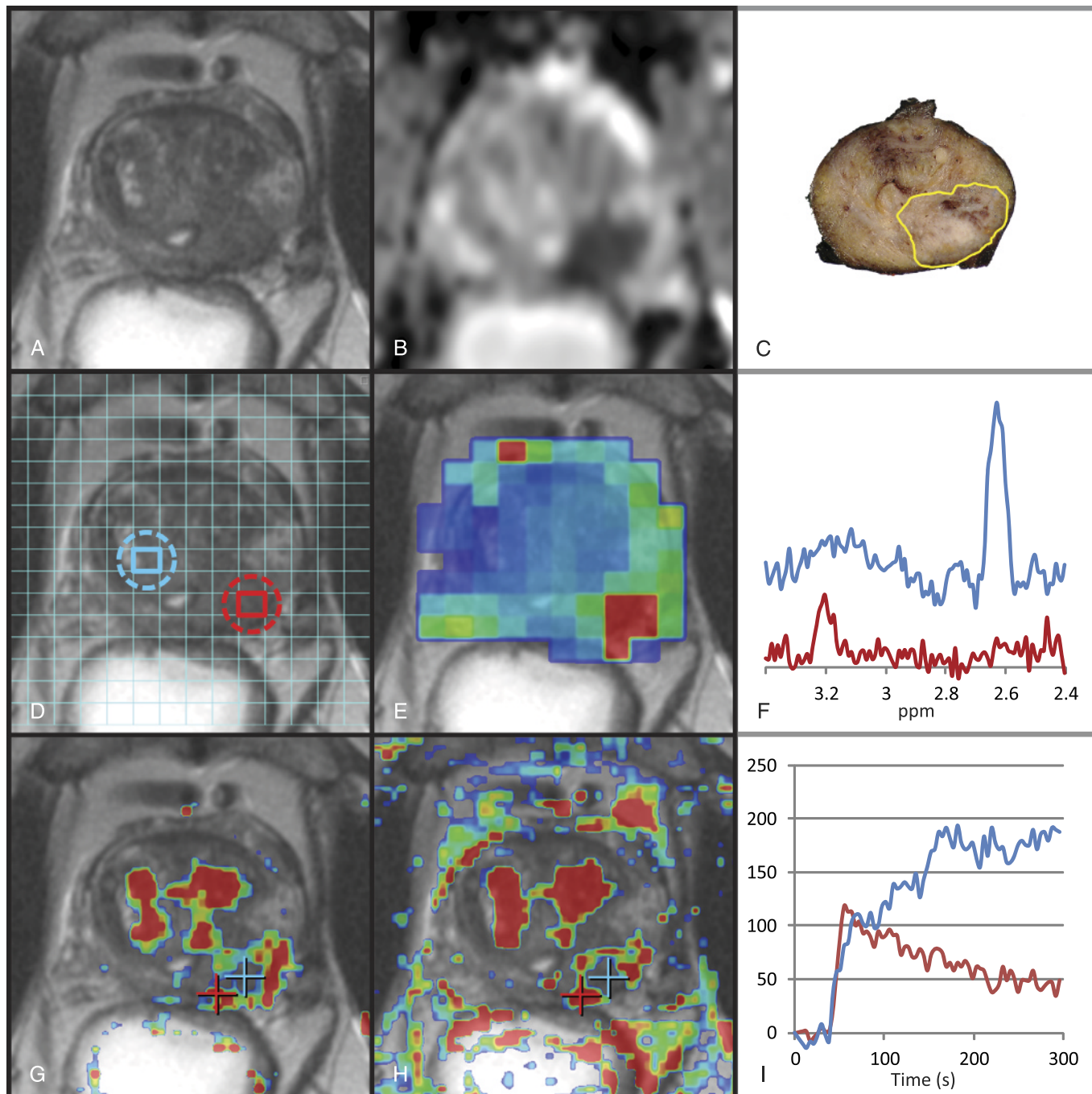
FIGURE 2. Example data set of a 69-year-old man with a Gleason 4 + 4 adenocarcinoma in the left peripheral zone. A, Transverse T2-weighted MRI scan shows a hypointense region in the left PZ. B, The corresponding apparent diffusion coefficient map shows a decreased ADC in the same region (minimum ADC approximately 600 μm^2/s). C, Macroscopic histology slide at the same level of the prostate, with the tumor identified by the pathologist (yellow outline). D, MRSI grid superimposed on T2-weighted image. The voxels corresponding to the spectra shown in F are outlined in blue and red; the dashed circles indicate the approximate true MRSI voxel size. E, (choline + spermine + creatine)/citrate map showing an increased metabolite ratio in the tumor region. F, Spectra corresponding to the voxels outlined in D. The noncancer spectrum (blue curve and blue outline in D) shows a high citrate signal and no distinguishable choline peak. In the tumor, only choline is observed, whereas all other metabolites are below the detection limit. Both spectra are identically scaled. G, Washin map. H, Washout map. I, Time-intensity curves of 2 voxels within the tumor. The boundary of the tumor shows a rapid washin and a rapid washout (red curve and red markers in G and H), whereas the central part of the tumor shows a slower, and continuing washin after the first pass of the bolus (blue curve and blue markers in G and H).

GG1–2 and GG3–5 were assessed using mixed model analyses and ROC analyses with patient-level bootstrapping to account for within-patient correlations.

The performance of combinations of parameters in discriminating between cancer and noncancer tissues, between GG1 and GG2–5 PZ cancers, as well as between GG1–2 and GG3–5 PZ cancers was assessed using the subset of ROIs for which all MR data was available, by logistic regression modeling (LRM) using generalized estimating equations to account for within-patient correlations.[23] Model selection

was based on the corrected quasi-likelihood under independence model criterion.[24] The performance of the models was evaluated using ROC analyses, again with patient-level bootstrapping to account for within-patient correlations. All statistical analyses were performed using SPSS for Windows version 22 (IBM, Armonk, NY).

RESULTS

Sixty-five PCa lesions greater than 0.5 cm^3 were found and annotated on histopathology (PZ, 47; TZ, 18) in 50 patients. Complete
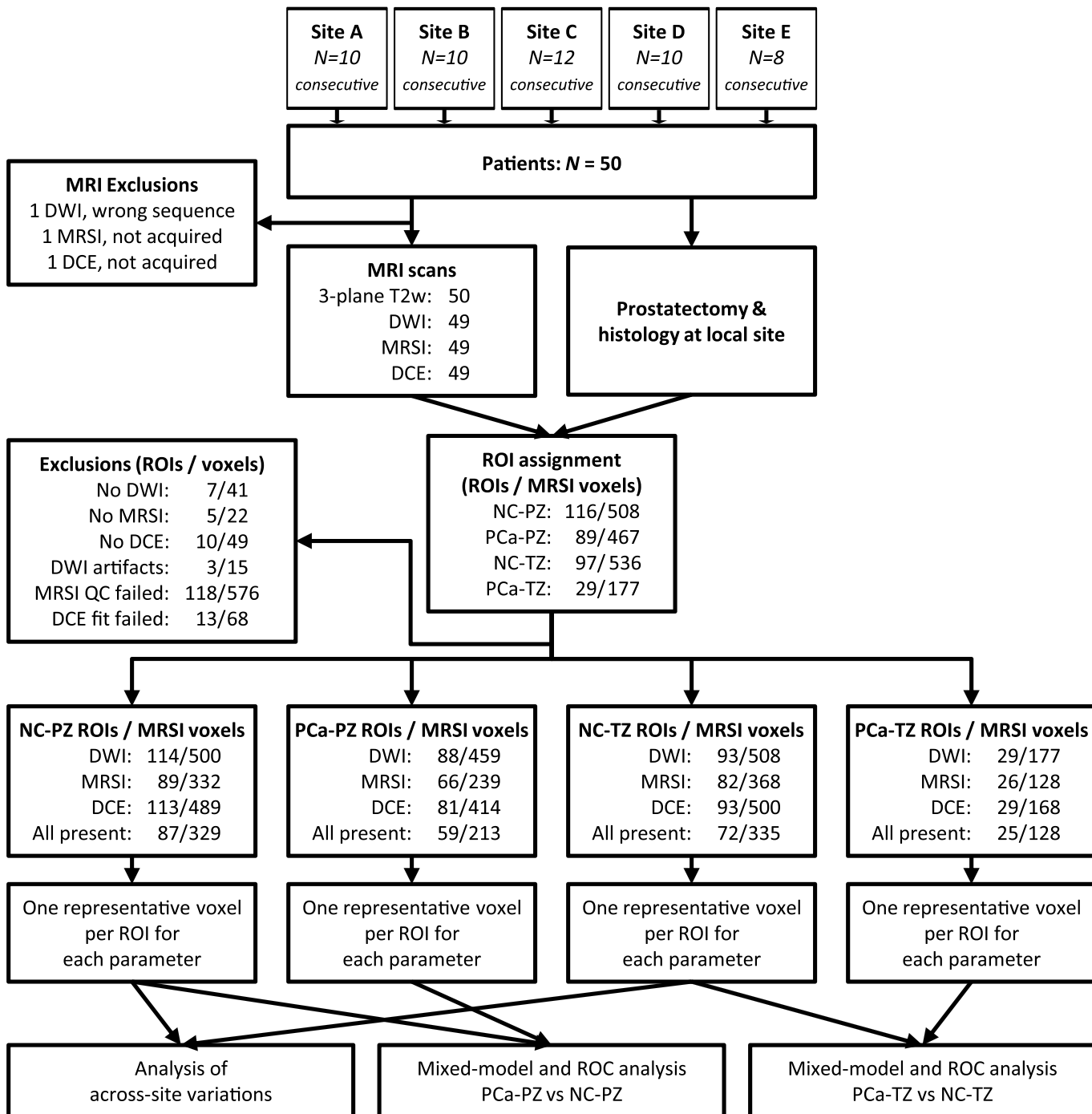
FIGURE 3. Flowchart of patients and data sets used in each analysis. NC-PZ indicates noncancer peripheral zone; PCa-PZ, cancer peripheral zone; NC-TZ, noncancer transition zone; PCa-TZ, cancer transition zone.

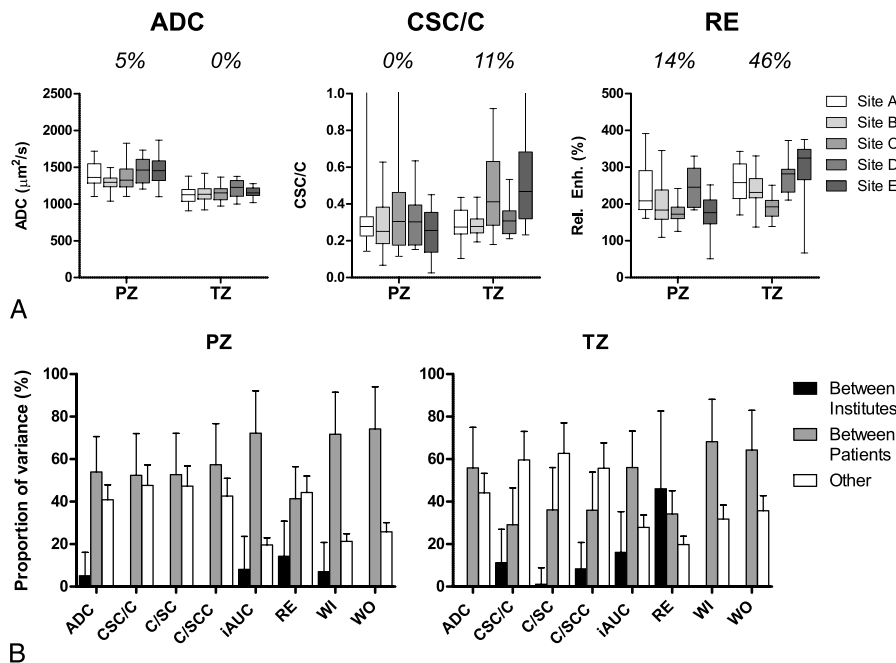**FIGURE 4.** Variance components analysis in noncancer tissues. A, Example boxplots of parameters derived from DWI, MRSI, and DCE, separated by institution. Boxes indicate the 25th, 50th, and 75th percentiles, and whiskers indicate minimum and maximum values. The percentages indicate the proportion of the total variance explained by differences between institutions. B, Proportion of the total variance explained by differences between institutions (black), between patients (gray), and other variations (within-patient variations and measurement fluctuations; white). Error bars indicate standard errors. ADC, apparent diffusion coefficient; CSC/C, (choline + spermine + creatine)/citrate; C/SC, choline/(spermine + creatine); C/SCC, choline/(spermine + creatine + citrate); iAUC, initial area under the gadolinium enhancement curve; RE, relative enhancement; WI, washin; WO, washout; PZ, peripheral zone; TZ, transition zone.

MRI datasets were acquired in 47/50 patients (representative example in Fig. 2), and a total of 331 ROIs consisting of 1688 MRSI voxels were annotated (average number of voxels per ROI, 5.1). Due to missing data or artifacts, not all MR parameters could be calculated in all ROIs: an overview of ROIs and MRSI voxels used in each analysis and tissue type is presented in Figure 3.

Across-Center Variations in Noncancer Tissues

The standardized mpMRI protocol yielded low variations across institutions (Fig. 4). The largest variation between institutions was found for RE (DCE) in noncancer TZ, for which the POV explained by differences between institutions was 46%. For all other parameters,

TABLE 3. Statistical Analysis of Differences in mpMRI Parameters Between Cancer and Noncancer Tissues

| | PZ | | | | | TZ | | | | |
| | Noncancer | | Cancer | | | Noncancer | | Cancer | | |
	Median	IQR	Median	IQR	*P*	Median	IQR	Median	IQR	*P*
ADC 25p*	1.35	[1.27–1.49]	1.02	[0.87–1.14]	<0.0005	1.18	[1.11–1.28]	0.99	[0.85–1.08]	<0.0005
CSC/C	0.28	[0.18–0.37]	0.40	[0.30–0.62]	0.001	0.30	[0.23–0.39]	0.35	[0.25–0.52]	0.064
C/SC	0.66	[0.44–1.04]	1.19	[0.75–2.66]	<0.0005	0.79	[0.47–1.12]	0.88	[0.66–1.77]	0.448
C/SCC	0.09	[0.05–0.13]	0.17	[0.11–0.29]	<0.0005	0.11	[0.07–0.15]	0.13	[0.08–0.21]	0.136
iAUC 75p	11.2	[8.2–15.0]	16.4	[11.1–19.1]	<0.0005	12.9	[10.5–18.6]	14.7	[11.9–18.4]	0.211
RE 75p	1.88	[1.63–2.29]	2.20	[1.83–2.70]	<0.0005	2.50	[2.10–2.96]	2.25	[1.98–2.51]	<0.0005
WI 75p†	12.8	[7.8–17.4]	17.6	[10.4–24.4]	<0.0005	16.8	[11.4–22.5]	17.9	[12.9–21.2]	0.267
WO 25p‡	−4.6	[−11.8 to −1.6]	−8.4	[−17.3 to −2.2]	<0.0005	−8.8	[−16.4 to −2.4]	−12.6	[−14.9 to −3.5]	0.501

P values represent the significance of the effect of malignancy on the mpMRI parameter in linear mixed modeling.

*Data are in units of 10^{-3} mm^2/s.

†Data are in units of % of prebolus signal intensity per second.

‡Data are in units of % of prebolus signal intensity per minute.

mpMRI indicates multiparametric magnetic resonance imaging; PZ, peripheral zone; TZ, transition zone; ADC, apparent diffusion coefficient; CSC/C, (choline + spermine + creatine)/citrate; C/SC, choline/(spermine + creatine); C/SCC, choline/(spermine + creatine + citrate); iAUC, initial area under the gadolinium enhancement curve; IQR, interquartile range; RE, relative enhancement; WI, washin; WO, washout; 25p, 25th percentile within sphere; 75p, 75th percentile within sphere.

TABLE 4. ROC Analysis Discriminating Cancer from Noncancer Tissue

	PZ		TZ	
	AUC	Sig.	AUC	Sig.
ADC 25p	0.93 ± 0.04	***	0.86 ± 0.10	***
CSC/C	0.73 ± 0.09	***	0.58 ± 0.14	0.143
C/SC	0.76 ± 0.09	***	0.60 ± 0.14	0.078
C/SCC	0.78 ± 0.08	***	0.58 ± 0.16	0.150
iAUC 75p	0.71 ± 0.09	***	0.56 ± 0.13	0.178
RE 75p	0.63 ± 0.11	***	0.63 ± 0.14	*
WI 75p	0.66 ± 0.11	**	0.56 ± 0.14	0.190
WO 25p	0.58 ± 0.10	0.058	0.57 ± 0.13	0.130
LRM†	0.93 ± 0.05	***	0.87 ± 0.09	***

*$P < 0.05$; **$P < 0.01$; ***$P < 0.001$.

†Logistic regression models included parameters ADC, C/SCC, and iAUC in the PZ and ADC, C/SC, and RE in the TZ.

ROC indicates receiver operator characteristic; PZ, peripheral zone; TZ, transition zone; ADC, apparent diffusion coefficient; CSC/C, (choline + spermine + creatine)/citrate; C/SC, choline/(spermine + creatine); C/SCC, choline/(spermine + creatine + citrate); iAUC, initial area under the gadolinium enhancement curve; IQR, interquartile range; RE, relative enhancement; WI, washin; WO, washout; 25p, 25th percentile within sphere; 75p, 75th percentile within sphere; LRM, logistic regression modeling.

the POV between institutions was less than 20%, both in noncancer PZ and TZ. The percentage of outliers removed in the VCA in PZ were 3.3% (median) and 6.2% (maximum, corresponding to 7/113 for RE). Median and maximum percentage of removed outliers in TZ were 2.7% and 8.5% (7/82, CSC/C). MRSI fits passed automatic and manual QC in 66% (1092/1666) of all voxels. The quality of MRSI varied significantly between institutions: the percentages of good quality voxels were 69% (268/390), 63% (200/319), 73% (326/449), 79% (224/282), and 33% (74/226) for institutions A through E, respectively ($P < 0.0005$).

Differences Between Cancer and Noncancer Tissues

Differences between cancer and noncancer PZ were highly significant for all investigated parameters (Table 3). The difference between cancer and noncancer TZ was also highly significant for the ADC, but much less so for MRSI and DCE parameters.

The best separation between cancer and noncancer tissue was achieved using the ADC, both in PZ (mean [95% confidence interval] AUC, 0.93 [0.89–0.96]) and in TZ (AUC, 0.86 [0.75–0.94]; Table 4, Fig. 5A). Logistic regression models yielded no significant additional discriminatory performance over ADC alone in either PZ or TZ: models including ADC, C/SCC, and iAUC in the PZ and ADC, C/SC, and RE in the TZ reached AUCs of 0.93 [0.88–0.97] and 0.87 [0.77–0.96], respectively.

Associations With Tumor Grade Groups in PZ

Almost all individual mpMRI parameters showed significant correlations with tumor grade group (Table 5). The strongest association was found with ADC (Spearman $r = -0.39$, $P < 0.001$). The MRSI and DCE parameters with the strongest association with GG were CSC/C ($r = 0.36$, $P < 0.01$) and WI ($r = 0.33$, $P < 0.01$), respectively.

In discriminating tumors with GG1 from those with GG2–5, linear mixed modeling (LMM) of individual parameters revealed a significant effect only for ADC ($P < 0.01$). This was consistent with ROC analysis: the highest AUC was obtained with ADC (mean [95% confidence interval] AUC, 0.74 [0.57–0.90]; $P < 0.001$), whereas none of the other parameters had AUCs significantly greater than 0.5. Logistic

regression modeling yielded no significant additional discriminatory performance over ADC alone: a model including parameters ADC, CSC/C, iAUC, and WI yielded an AUC of 0.78 [0.60–0.90] (Table 5, Fig. 5B).

In discriminating tumors with GG1–2 from those with GG3–5, LMM of individual parameters showed significant effects for ADC ($P < 0.01$), C/SC ($P < 0.05$), and WI ($P < 0.05$). In ROC analysis, all parameters except C/SCC and WO yielded AUCs significantly greater than 0.5. Nevertheless, their discriminatory performance was moderate: the highest AUC, obtained with C/SC, was 0.72 [0.56–0.85], with ADC and WI showing AUCs of 0.70 [0.55–0.85] and 0.71 [0.54–0.85], respectively. An LRM including parameters ADC, C/SC, iAUC, and WI improved the AUC for discrimination between GG1–2 and GG3–5 to 0.89 [0.78–0.98]; however, this was not significantly higher than the AUC of any of the individual parameters (Table 5, Fig. 5B).

DISCUSSION

This work presents the first quantitative prostate mpMRI multicenter trial at 3 T, the current state-of-the-art in PCa imaging. Although the technique, interpreted in a qualitative way by radiologists, has been successfully validated in 2 large multicenter trials for guiding biopsies in men with high prostate specific antigen levels,[4,5] full quantitation of mpMRI offers opportunities not only to detect PCa, but also to assess its aggressiveness and its progression over time. Interestingly, quantitative parameters are not incorporated in current guidelines, but have been suggested for use in future versions if intersite differences can be overcome or quantified.[8,11] Our study represents an important step toward the implementation of large-scale prospective and quantitative multicenter studies with a standardized data acquisition and postprocessing protocol. Although many single-center studies have demonstrated the added value of using one or several functional MR techniques to detect, localize, and characterize PCa, a lack of standardization has complicated comparison of results between different institutions and studies as well as quality control.

Our results show that complete standardization of acquisition and postprocessing protocols leads to quantitative functional parameter values that are very similar across multiple sites in noncancer tissues. Variation in the parameters is not caused by variation between institutes, ruling out site-specific differences in histopathological description of noncancer tissues. Instead, variation was mostly caused by interpatient variability, for example due to natural variation and benign disease differences between patients, and by intrapatient variations, which in this case represent variations between different locations within the same prostatic zone in the same patient. Both of these may also include effects of the presence of cancer in the prostate on nearby noncancer tissue (edema, tiny tumor infiltrates, blood flow effects, etc). The quantitative functional parameter values enabled separation between cancer and noncancer tissues, as well as discriminating between cancer grade groups with pooled multicenter data comparable to that reported in single-center studies.[25–30] This means that it is feasible to use fixed thresholds across multiple institutions to differentiate cancer from noncancer tissues in patients with biopsy-proven PCa without compromising the discriminative performance of these parameters. This is a prerequisite for incorporating quantitative parameter thresholds in multicenter predictive studies of tumor location and grade group as well as in clinical guidelines for tumor localization and assessment using mpMRI. Quantitative thresholds can help decrease the subjective interpretation of mpMRI of the prostate, which currently results in only moderate interobserver agreement between readers of the same data,[9,31] and will facilitate the use of computer-aided diagnosis systems. It may also enable a more objective follow-up of patients under active surveillance or during treatment, but this would also require an analysis of the repeatability and reproducibility of the quantitative parameters,[32] which was not part of the present study.
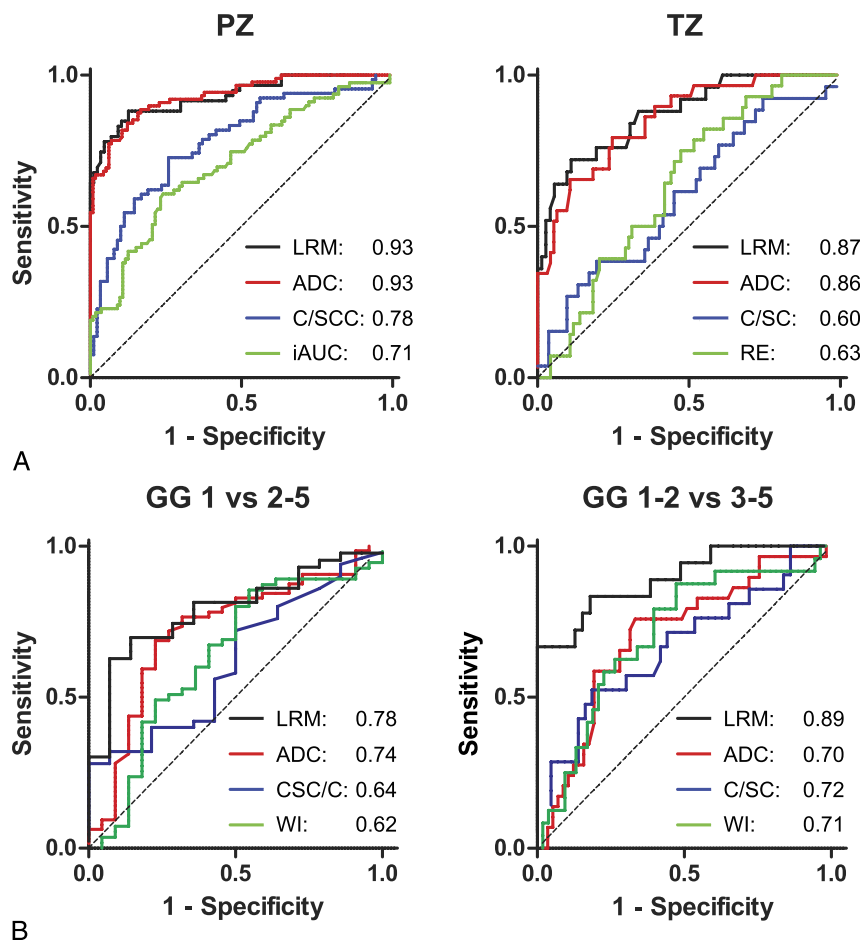
FIGURE 5. ROC analyses. A, Separation between nonmalignant and malignant tissues in PZ as well as TZ. B, Separation between grade group 1 versus grade groups 2 to 5 PZ tumors, as well as between grade groups 1–2 versus grade groups 3–5. In each plot, the ROC curve of the best performing individual parameter derived from each acquisition method, as well as that of the logistic regression model are shown. Numbers indicate the mean AUC obtained from 10,000-fold patient-level bootstrapping.

Although the high degree of standardization used in this study might not be realistically achievable on a full clinical scale, for example, involving a variety of systems and vendors, our results may be used to assess what degree of standardization would be required in multicenter studies and clinical guidelines. For instance, in preparation for nonstandardized studies, preliminary data may be used to quantify variations between patients and institutions and to compare them to those found in this work. This will enable investigators to assess whether protocol changes at one or more of the participating institutions may be useful to reduce interinstitutional variation. Diffusion-weighted imaging yielded good separation between PCa and noncancer tissues in both PZ and TZ, with mean AUC of 0.93 and 0.86, respectively. The added value of ADC for tumor localization is indeed well established in the PZ.[13,33,34] In the TZ, however, the advantage is not as clear: previous histology-referenced ROI studies have reported similar results as those shown here, but reader-based localization studies have not clearly demonstrated an added value of ADC in the TZ.[35–37] Consequently, the T2w image series is the most dominant sequence for the TZ in the recent version of the Prostate Imaging Reporting and Data System (PI-RADS v2).[8,38] It remains unknown what causes this discrepancy, but our results suggest that incorporating quantitative ADC thresholds into the reading strategy might improve localization accuracy in the TZ. However, the number of TZ tumor foci in our study was low.

Adding information from MRSI and DCE-derived parameters to the ADC maps using logistic regression did not improve separation between cancer and noncancer tissue. This agrees with earlier studies: although several studies have reported strongly improved localization accuracies for both MRSI and DCE compared with T2w alone,[39,40] an incremental value of these methods over ADC has not been firmly established.[41,42] This may be attributable to several factors. For instance, all measurements were performed without an endorectal coil. The associated SNR reduction led to a lower overall spectral quality, illustrated by a decreased number of voxels passing quality control.[21] This was partially compensated by using a larger voxel size, which however also increased partial volume effects. Spectral quality was also affected by operator experience at the local sites, illustrated by the large between-site differences in the number of QC-passed voxels. MRSI could only be considered for reintroduction into the PIRADS system if voxel failure rates get smaller and less dependent on local expertise. For DCE analysis, we only used semiquantitative parameters to obtain quantities independent of any model assumptions. It may be that pharmacokinetic modeling with patient-specific arterial input functions would reduce the large between-patient variations; however, determining the arterial input functions and the quantitative precontrast T1-maps needed for pharmacokinetic modeling would also introduce additional variations, possibly offsetting this advantage. Finally,

TABLE 5. Statistical Analysis of Associations Between mpMRI and Cancer Aggressiveness in the PZ

| | Spearman Correlation With Grade Group | | Separation of Grade Groups 1 vs 2–5 | | | Separation of Grade Groups 1–2 vs 3–5 | | |
| | | | LMM | ROC Analysis | | LMM | ROC Analysis | |
	r	Sig.	Sig.	AUC	Sig.	Sig.	AUC	Sig.
ADC 25p	−0.39	***	**	0.74 ± 0.16	***	**	0.70 ± 0.15	**
CSC/C	0.36	**	NS	0.64 ± 0.19	NS	NS	0.70 ± 0.18	*
C/SC	0.18	NS	NS	0.56 ± 0.22	NS	*	0.72 ± 0.15	**
C/SCC	0.32	*	NS	0.57 ± 0.18	NS	NS	0.66 ± 0.19	NS
iAUC 75p	0.24	*	NS	0.59 ± 0.20	NS	NS	0.67 ± 0.17	*
RE 75p	0.24	*	NS	0.54 ± 0.29	NS	NS	0.69 ± 0.17	*
WI 75p	0.33	**	NS	0.62 ± 0.24	NS	*	0.71 ± 0.15	**
WO 25p	−0.13	NS	NS	0.56 ± 0.19	NS	NS	0.57 ± 0.18	NS
LRM†	—	—	—	0.78 ± 0.15	**	—	0.89 ± 0.10	***

*$P < 0.05$; **$P < 0.01$; ***$P < 0.001$.

†Logistic regression models included parameters ADC, CSC/C, iAUC, and WI for separating tumor grade groups 1 from 2–5, and parameters ADC, C/SC, iAUC, and WI for separating grade groups 1–2 from 3–5.

mpMRI indicates multiparametric magnetic resonance imaging; PZ, peripheral zone; LMM, linear mixed modeling; ROC, receiver operator characteristic; ADC, apparent diffusion coefficient; CSC/C, (choline + spermine + creatine)/citrate; C/SC, choline/(spermine + creatine); C/SCC, choline/(spermine + creatine + citrate); iAUC, initial area under the gadolinium enhancement curve; IQR, interquartile range; RE, relative enhancement; WI, washin; WO, washout; 25p, 25th percentile within sphere; 75p, 75th percentile within sphere; LRM, logistic regression modeling; NS, not significant.

regions of benign disease such as BPH were not indicated on histopathology, and no attempt was made to place noncancer ROIs outside of such regions. This especially affected DCE results in the TZ, which is known to have enhancing BPH nodules, and contributed to the large variation in DCE results in this zone.

Quantitative parameters derived from each of the functional imaging methods were found to correlate with tumor grade group in the PZ, and also the separation between tumor grade groups in this multicenter dataset, as quantified in ROC analysis, was comparable to previously published single-center studies.[21,43] For separating GG1 from higher-grade groups in PZ tumors, the ADC was found to be the best performing individual parameter, and adding information from MRSI and DCE by LRM modeling did not appreciably improve this performance. However, for separating higher-grade group (ie, GG ≥ 3) PZ tumors from lower and intermediate ones (ie, GG ≤ 2), combining parameters from DWI, MRSI, and DCE by LRM did result in a substantially higher area under the ROC curve than found with any of the individual parameters. Although this improvement was not statistically significant, this suggests that MRSI and/or DCE may have additional value in separating high-grade group PZ tumors from low to intermediate ones. This should be validated in a different and larger patient cohort that better reflects the clinical reality of not only localizing and grading biopsy-proven cancers, but also detecting possible cancers.

Special attention was paid to the methodology of ROI placement and matching between MRI and histopathology in this study. Histopathologic analysis was performed locally at each site only, and no centralized analysis was performed. Therefore, variability in sample preparation and interreader variability between pathologists, which likely influences the discriminatory performance of these multicenter mpMRI data,[44] could not be quantified. Furthermore, advanced methods for correlating histopathology to MRI[45] were not available. To overcome these challenges, we used a method of ROI placement minimizing the effect of spatial mismatch on the results. No attempt was made to fully delineate entire tumor or nontumor regions on MRI scans; instead, only ROIs with a high certainty of residing within the intended tissue type were defined using only histopathology and T2w MRI scans. This avoided bias of drawing ROIs on suspicious regions in functional parameter maps. Furthermore, we designed our method to be sensitive to the hot spots that are often observed in functional parameter maps

in PCa tissue, which are arguably most representative of tissue abnormality, but are typically smaller than our unit of ROI definition (spheres of MRSI voxel size). The histogram analysis performed in each sphere (with 25th and 75th percentiles of functional parameter values) allowed to capture these hot spots, rather than assuming a symmetric distribution of parameter values.[46] By including multiple overlapping spheres in each ROI and selecting only the most aberrant value (ie, highest metabolite ratio, lowest 25th percentile, or highest 75th percentile) out of these spheres for each parameter separately, our approach accounted for the fact that hot spots in PCa tissue may be found at different locations in different parameter maps. Biasing tumors to more extreme values was avoided by following this same approach in cancer as well as in noncancer tissues. Finally, restricting the maximum number of spheres in each ROI to 7 reduced biases induced by differing ROI sizes, as larger ROIs are intrinsically more likely to contain extreme values. A drawback of this approach is that known confounding features that can be recognized by experienced radiologists (eg, symmetrical contrast enhancement in the transition zone, contrast-enhancing BPH nodules, or sharply demarcated benign lesions on T2w images) are not excluded from noncancer tissue. The combination of radiological experience with a quantitative mpMRI approach might ultimately prove to be the best solution toward PCa detection, localization, and grade group assessment. Whether translation of the mpMRI methods to ultrahigh magnetic field strengths[47] could further improve this is a direction of future research.

In conclusion, standardized data acquisition and postprocessing protocols in prostate mpMRI at 3 T can produce equivalent quantitative results across multiple institutions in a single-vendor setting. Standardized quantitative multicenter mpMRI data can separate PCa from noncancer tissues and discriminate between cancer grade groups similarly well as previously reported single-center data, which is an important step toward objective or automated interpretation of prostate mpMRI examinations.

REFERENCES

1. Bray F, Ferlay J, Soerjomataram I, et al. Global cancer statistics 2018: GLOBOCAN estimates of incidence and mortality worldwide for 36 cancers in 185 countries. *CA Cancer J Clin.* 2018;68:394–424.

2. Hoeks CM, Barentsz JO, Hambrock T, et al. Prostate cancer: multiparametric MR imaging for detection, localization, and staging. *Radiology.* 2011;261:46–66.

3. Scheenen TW, Rosenkrantz AB, Haider MA, et al. Multiparametric magnetic resonance imaging in prostate cancer management: current status and future perspectives. *Invest Radiol.* 2015;50:594–600.

4. Ahmed HU, El-Shater Bosaily A, Brown LC, et al. Diagnostic accuracy of multiparametric MRI and TRUS biopsy in prostate cancer (PROMIS): a paired validating confirmatory study. *Lancet.* 2017;389:815–822.

5. Kasivisvanathan V, Rannikko AS, Borghi M, et al. MRI-targeted or standard biopsy for prostate-cancer diagnosis. *N Engl J Med.* 2018;378:1767–1777.

6. van der Leest M, Cornel E, Israël B, et al. Head-to-head comparison of transrectal ultrasound-guided prostate biopsy versus multiparametric prostate resonance imaging with subsequent magnetic resonance-guided biopsy in biopsy-naïve men with elevated prostate-specific antigen: a large prospective multicenter clinical study. *Eur Urol.* 2018.

7. Mottet N, Bellmunt J, Bolla M, et al. EAU-ESTRO-SIOG guidelines on prostate cancer. part 1: screening, diagnosis, and local treatment with curative intent. *Eur Urol.* 2017;71:618–629.

8. Weinreb JC, Barentsz JO, Choyke PL, et al. PI-RADS prostate imaging - reporting and data system: 2015, version 2. *Eur Urol.* 2016;69:16–40.

9. Rosenkrantz AB, Ginocchio LA, Cornfeld D, et al. Interobserver reproducibility of the PI-RADS version 2 lexicon: a multicenter study of six experienced prostate radiologists. *Radiology.* 2016;280:793–804.

10. Dickinson L, Ahmed HU, Allen C, et al. Magnetic resonance imaging for the detection, localisation, and characterisation of prostate cancer: recommendations from a european consensus meeting. *Eur Urol.* 2011;59:477–494.

11. Barentsz JO, Weinreb JC, Verma S, et al. Synopsis of the PI-RADS v2 guidelines for multiparametric prostate magnetic resonance imaging and recommendations for use. *Eur Urol.* 2016;69:41–49.

12. Polanec SH, Helbich TH, Bickel H, et al. Quantitative apparent diffusion coefficient derived from diffusion-weighted imaging has the potential to avoid unnecessary MRI-guided biopsies of mpMRI-Detected PI-RADS 4 and 5 lesions. *Invest Radiol.* 2018;53:736–741.

13. He D, Chatterjee A, Fan X, et al. Feasibility of dynamic contrast-enhanced magnetic resonance imaging using low-dose gadolinium: comparative performance with standard dose in prostate cancer diagnosis. *Invest Radiol.* 2018;53:609–615.

14. Wright AJ, Kobus T, Selnaes KM, et al. Quality control of prostate 1H MRSI data. *NMR Biomed.* 2013;26:193–203.

15. Provencher SW. Estimation of metabolite concentrations from localized in vivo proton NMR spectra. *Magn Reson Med.* 1993;30:672–679.

16. Huisman HJ, Engelbrecht MR, Barentsz JO. Accurate estimation of pharmacokinetic contrast-enhanced dynamic MRI parameters of the prostate. *J Magn Reson Imaging.* 2001;13:607–614.

17. Epstein JI, Zelefsky MJ, Sjoberg DD, et al. A contemporary prostate cancer grading system: a validated alternative to the Gleason score. *Eur Urol.* 2016;69:428–435.

18. McNeal JE, Redwine EA, Freiha FS, et al. Zonal distribution of prostatic adenocarcinoma. Correlation with histologic pattern and direction of spread. *Am J Surg Pathol.* 1988;12:897–906.

19. Augustin H, Hammerer PG, Graefen M, et al. Insignificant prostate cancer in radical prostatectomy specimen: time trends and preoperative prediction. *Eur Urol.* 2003;43:455–460.

20. Scheenen TW, Klomp DW, Röll SA, et al. Fast acquisition-weighted three-dimensional proton MR spectroscopic imaging of the human prostate. *Magn Reson Med.* 2004;52:80–88.

21. Kobus T, Vos PC, Hambrock T, et al. Prostate cancer aggressiveness: in vivo assessment of MR spectroscopy and diffusion-weighted imaging at 3 T. *Radiology.* 2012;265:457–467.

22. Tukey JW. *Exploratory Data Analysis.* Reading, MA: Addison-Wesley; 1977.

23. Zeger SL, Liang KY. Longitudinal data analysis for discrete and continuous outcomes. *Biometrics.* 1986;42:121–130.

24. Pan W. Akaike's information criterion in generalized estimating equations. *Biometrics.* 2001;57:120–125.

25. Hambrock T, Somford DM, Huisman HJ, et al. Relationship between apparent diffusion coefficients at 3.0-T MR imaging and Gleason grade in peripheral zone prostate cancer. *Radiology.* 2011;259:453–461.

26. Kobus T, Hambrock T, Hulsbergen-van de Kaa CA, et al. In vivo assessment of prostate cancer aggressiveness using magnetic resonance spectroscopic imaging at 3 T with an endorectal coil. *Eur Urol.* 2011;60:1074–1080.

27. Selnæs KM, Heerschap A, Jensen LR, et al. Peripheral zone prostate cancer localization by multiparametric magnetic resonance at 3 T. *Invest Radiol.* 2012;47:624–633.

28. Vos EK, Litjens GJ, Kobus T, et al. Assessment of prostate cancer aggressiveness using dynamic contrast-enhanced magnetic resonance imaging at 3 T. *Eur Urol.* 2013;64:448–455.

29. Le JD, Tan N, Shkolyar E, et al. Multifocality and prostate cancer detection by multiparametric magnetic resonance imaging: correlation with whole-mount histopathology. *Eur Urol.* 2015;67:569–576.

30. Hoang Dinh A, Melodelima C, Souchon R, et al. Quantitative analysis of prostate multiparametric MR images for detection of aggressive prostate cancer in the peripheral zone: a multiple imager study. *Radiology.* 2016;280:117–127.

31. Muller BG, Shih JH, Sankineni S, et al. Prostate cancer: interobserver agreement and accuracy with the revised prostate imaging reporting and data system at multiparametric MR imaging. *Radiology.* 2015;277:741–750.

32. Fedorov A, Vangel MG, Tempany CM, et al. Multiparametric magnetic resonance imaging of the prostate: repeatability of volume and apparent diffusion coefficient quantification. *Invest Radiol.* 2017;52:538–546.

33. Haider MA, van der Kwast TH, Tanguay J, et al. Combined T2-weighted and diffusion-weighted MRI for localization of prostate cancer. *AJR Am J Roentgenol.* 2007;189:323–328.

34. Lim HK, Kim JK, Kim KA, et al. Prostate cancer: apparent diffusion coefficient map with T2-weighted images for detection—a multireader study. *Radiology.* 2009;250:145–151.

35. Hoeks CM, Vos EK, Bomers JG, et al. Diffusion-weighted magnetic resonance imaging in the prostate transition zone: histopathological validation using magnetic resonance-guided biopsy specimens. *Invest Radiol.* 2013;48:693–701.

36. Jung SI, Donati OF, Vargas HA, et al. Transition zone prostate cancer: incremental value of diffusion-weighted endorectal MR imaging in tumor detection and assessment of aggressiveness. *Radiology.* 2013;269:493–503.

37. Kitajima K, Takahashi S, Ueno Y, et al. Clinical utility of apparent diffusion coefficient values obtained using high b-value when diagnosing prostate cancer using 3 tesla MRI: Comparison between ultra-high b-value (2000 s/mm^2) and standard high b-value (1000 s/mm^2). *J Magn Reson Imaging.* 2012;36:198–205.

38. Barentsz J, de Rooij M, Villeirs G, et al. Prostate Imaging-Reporting and Data System Version 2 and the implementation of high-quality prostate magnetic resonance imaging. *Eur Urol.* 2017;72:189–191.

39. Fütterer JJ, Heijmink SW, Scheenen TW, et al. Prostate cancer localization with dynamic contrast-enhanced MR imaging and proton MR spectroscopic imaging. *Radiology.* 2006;241:449–458.

40. Turkbey B, Pinto PA, Mani H, et al. Prostate cancer: value of multiparametric MR imaging at 3 T for detection—histopathologic correlation. *Radiology.* 2010;255:89–99.

41. Kitajima K, Kaji Y, Fukabori Y, et al. Prostate cancer detection with 3 T MRI: Comparison of diffusion-weighted imaging and dynamic contrast-enhanced MRI in combination with T2-weighted imaging. *J Magn Reson Imaging.* 2010;31:625–631.

42. Mazaheri Y, Shukla-Dave A, Hricak H, et al. Prostate cancer: identification with combined diffusion-weighted MR imaging and 3D 1H MR spectroscopic imaging—correlation with pathologic findings. *Radiology.* 2008;246:480–488.

43. Vos EK, Kobus T, Litjens GJ, et al. Multiparametric magnetic resonance imaging for discriminating low-grade from high-grade prostate cancer. *Invest Radiol.* 2015;50:490–497.

44. Netto GJ, Eisenberger M, Epstein JI, et al. Interobserver variability in histologic evaluation of radical prostatectomy between central and local pathologists: findings from TAX 3501 multinational clinical trial. *Urology.* 2011;77:1155–1160.

45. Costa DN, Chatzinoff Y, Passoni NM, et al. Improved magnetic resonance imaging-pathology correlation with imaging-derived, 3D-printed, patient-specific whole-mount molds of the prostate. *Invest Radiol.* 2017;52:507–513.

46. Donati OF, Mazaheri Y, Afaq A, et al. Prostate cancer aggressiveness: assessment with whole-lesion histogram analysis of the apparent diffusion coefficient. *Radiology.* 2014;271:143–152.

47. Lagemaat MW, Philips BW, Vos EK, et al. Feasibility of multiparametric magnetic resonance imaging of the prostate at 7 T. *Invest Radiol.* 2017;52:295–301.